

PACS numbers: 42.82.Cr; 42.82.Et; 42.70.Mp
DOI: 10.1070/QE2009v039n01ABEH013878

Optimisation of the proton-exchange technology for fabricating channel waveguides in lithium niobate crystals

I.V. Il'ichev, A.S. Kozlov, P.V. Gaenko, A.V. Shamrai

***Abstract*. We have studied the effect of process parameters on the mode profile in lithium niobate channel waveguides produced by low-temperature proton exchange. A model has been proposed for the processes underlying waveguide formation, and has been used to numerically calculate the mode profile for various fabrication parameters. We have identified low-temperature proton exchange conditions which ensure high electro-optical performance of the waveguides and stability towards fabrication errors. The obtained results may be helpful in optimising integrated optical devices and matching them to various types of optical fibres.**

Keywords: *integrated optics, proton exchange, lithium niobate.*

1. Introduction

Lithium niobate is widely used in integrated optics owing to its attractive electrooptical, acoustooptic, piezoelectric and photorefractive properties. Optical waveguides in lithium niobate crystals for integrated optical applications are commonly produced via low-temperature proton exchange followed by annealing [1]. The basic principle of this approach is that an $LiNbO_3$ substrate reacts with molten organic or inorganic acids at 180 – 250 °C, which leads to partial proton substitution for lithium ions in the surface layer of the substrate. This increases the extraordinary refractive index n_e of lithium niobate by $\sim 10^{-1}$ and reduces its ordinary index n_o by 10^{-2}, resulting in the formation of a near-surface waveguide layer for extraordinary wave propagation [2]. This hydrogen-enriched layer ($H_xLi_{1-x}NbO_3$) has a steplike geometric profile and is characterised by a relatively high ($0.5 < x < 0.7$) degree of exchange (crystallographic phases β_1, β_2, ...) [3]. The formation of waveguides is accompanied by degradation of the electro-optical properties of lithium niobate in the waveguide region [4].

Post-exchange annealing at 300 – 400 °C with no proton sources leads to diffusion broadening of the hydrogen-enriched layer towards the substrate bulk. Concurrently, the material undergoes structural phase transitions as a result of the reduction in local ion concentration. The resultant waveguide has a graded geometric profile and a relatively low ($x < 0.4$) proton concentration (phases α, k_1, and k_2). The annealed waveguide layer differs less in refractive indices from the substrate, $\Delta n_e \approx 10^{-2}$ and $\Delta n_o \approx -10^{-3}$, and is comparable in electrooptical properties to unprocessed lithium niobate [5]. The crystallographic phases and structural phase transitions of proton-exchanged $LiNbO_3$ waveguides were studied in detail by Korkishko et al. [6].

Previous detailed studies on the formation of proton-exchanged waveguides were concerned with planar waveguides and examined the proton concentration and refractive index profiles in the waveguide layer [1 – 8]. A planar waveguide has a one-dimensional (1D) cross-sectional structure, which is readily amenable to theoretical analysis. This allows one to accurately assess the index profile. Moreover, prism-coupling measurement of the index profile in planar waveguides is an established technique. In practical applications, however, use is mostly made of channel waveguides, which have a 2D cross-sectional structure. In most cases, theoretical analysis of their structure requires numerical calculations. In this work, we examine the formation of proton-exchanged channel waveguides.

A key characteristic of light propagating along a channel waveguide is its mode profile: the intensity distribution in the cross section perpendicular to the propagation direction. The mode profile plays a central role in determining the characteristics of integrated optical devices such as couplers and modulators. In particular, the optical loss through a connection between a single-mode channel waveguide and optical fibre is mainly due to the mode-profile mismatch between the waveguide and fibre.

The mode profile of an optical channel waveguide is determined by the 2D index distribution across the wave-

I.V. Il'ichev, A.S. Kozlov, P.V. Gaenko, A.V. Shamrai A.F. Ioffe Physical Technical Institute, Russian Academy of Sciences, Politekhnicheskaya ul. 26, 194021 St. Petersburg, Russia; e-mail: iiv@mail.ioffe.ru

Received 8 April 2008; revision received 29 July 2008
Kvantovaya Elektronika **39** (1) 98 – 104 (2009)
Translated by O.M. Tsarev

guide and, hence, depends strongly on the fabrication process.

The objective of this work was to study the effect of fabrication parameters on the mode profile and optical characteristics of single-mode proton-exchanged channel waveguides in lithium niobate crystals. Our main purpose was to develop an approach for optimising the fabrication of such waveguides via low-temperature proton exchange in order to achieve predetermined optical characteristics of integrated optical devices.

2. Experimental results

Sample fabrication. Single-mode channel waveguides for the 1530- to 1580-nm telecommunication window were fabricated on *x*-cut lithium niobate substrates by low-temperature proton exchange followed by air annealing. Metal (Al, Ti) masks having eight slits, with the slit width varying from 3 to 10 μm in 1-μm steps, were produced by photolithography and vacuum sputtering. The exchange process was run at temperatures from 180 to 200 °C for various lengths of time (20 min to 4 h), using molten benzoic acid as the proton source. The proton activity was controlled by lithium benzoate additions (0 – 5 wt %). After this step, the metal mask was removed by wet etching, the sample end-faces were polished, and the waveguides were air-annealed at 350 °C in several steps, with mode profile measurements after each step.

Mode profile measurements. Waveguide mode profiles were measured using a purpose-designed apparatus for optical probe microscopy (Fig. 1). The intensity distribution was probed by scanning a single-mode fibre (mode diameter of 5.8 μm) near the launch end of the waveguide in 0.4-μm steps. The probe positioning accuracy (40 nm) was checked by an optical interferometer. The intensity depth/width distribution thus obtained (Fig. 2) is a convolution of the known intensity distribution function of the fibre mode and that of the waveguide mode, and gives an idea of the near-field mode profile. From the intensity distribution, we assessed the width w_m and depth d_m of the waveguide mode (at a $1/e^2$ level). For simplicity, we assumed that the 2D intensity distribution is the product of *x*-axis (horizontal) and *y*-axis (vertical) distributions. The profiles along both axes were represented as a convolution of two Gaussians: the mode profile of the fibre probe (known dispersion coefficient $f = 2.9$ μm) and that of the channel waveguide (unknown dispersion coefficient $\sigma_{w,x(y)}$). The *x*- and *y*-axis dispersion coefficients of the waveguide mode profile may differ significantly. The scanning results for both axes were fitted by Gaussians, with least-squares dispersion coefficients $\sigma_{M,x(y)}$. The width and depth of the channel waveguide mode are given by $w_m = 2\sigma_{w,x}$ and $d_m = 2\sigma_{w,y}$. The unknown dispersion coefficients were determined using the relation $\sigma^2_{w,x(y)} = 2\sigma^2_{M,x(y)} - \sigma^2_f$. Note that the actual waveguide mode profile is non-Gaussian, so the mode width and depth extracted from scanning results are a rather rough approximation. Nevertheless, such experimentally determined values can be used to examine the influence of fabrication parameters on the channel waveguide mode profile and to compare modelling results with experimental data.

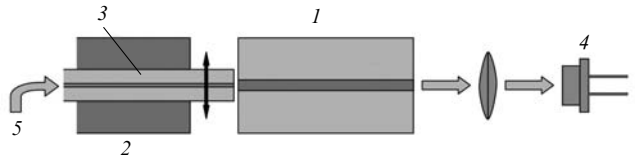

Figure 1. Experimental setup for optical probe microscopy: (*1*) sample; (*2*) piezoelectric three-axis positioning system with interferometric control; (*3*) single-mode 6-μm-core optical fibre; (*4*) photodetector; (*5*) 1550-nm radiation input. Scan step is 0.4 μm; probe positioning accuracy is 40 nm.

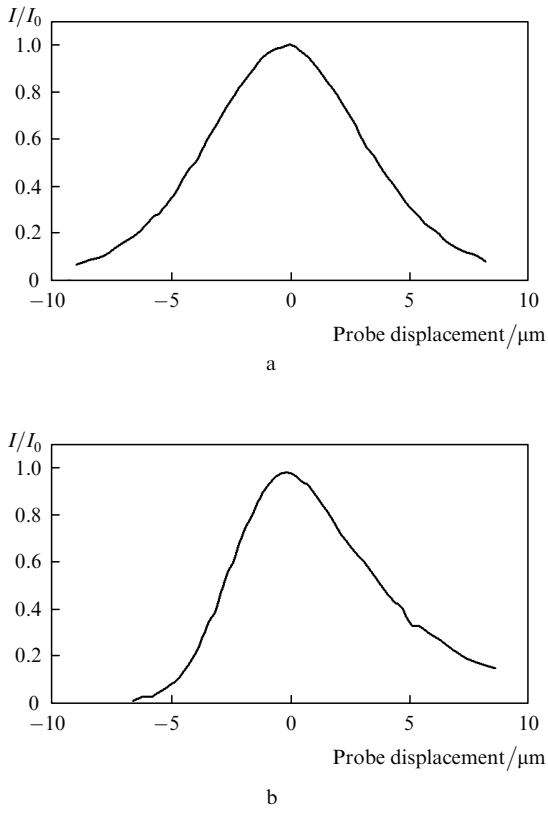

Figure 2. Measured normalised intensity (a) width and (b) depth profiles in a waveguide. Proton exchange time, 20 min; anneal time, 2 h; slit width in the mask, 8.2 μm.

Determination of electrooptical coefficients. The electro-optical coefficients of the waveguides were determined by measuring the half-wave voltage of the Fabry – Perot cavity formed by the waveguide end-faces. After annealing for more than 2 h, none of our samples showed significant electrooptical degradation: in all the waveguides, the effective electrooptical coefficient was 29 – 30 pm V^{-1} (that of bulk lithium niobate is $r_{33} = 32$ pm V^{-1}).

3. Model

The formation of waveguides during low-temperature proton exchange and the propagation of guided modes in the resultant waveguides were analysed using numerical simulation. The guided-mode region of the waveguide was divided into a 300×300 node grid with a grid spacing of

0.25 μm. For each node, we calculated the concentration of hydrogen ions, refractive indices and wave amplitude.

To describe the formation of channel waveguides during low-temperature proton exchange followed by air annealing, we consider two-step diffusion in the 2D geometry of the cross section of the substrate. The first step is proton exchange on the lithium niobate surface in molten benzoic acid. The second step is high-temperature annealing.

The first step creates a hydrogen-enriched zone with sharp boundaries (Fig. 3). In our model, this zone has a trapezoidal cross section. At the grid nodes within the trapezium, the hydrogen content is set to be $x = 0.55$, as is typical of proton exchange [3]. Beyond the trapezium, the hydrogen content is zero. The geometry of this zone is defined by the slit width s in the mask, and the proton diffusion length L. The latter depends on the proton exchange time t_1 and is given by [1]

$$L = 2\sqrt{D_1 t_1}, \tag{1}$$

where D_1 is the diffusion coefficient in the first step, which is a fitting parameter of the model (the diffusion coefficient was assumed to be isotropic). From an analysis of the first step, we derived the hydrogen ion distribution over the nodes, $X_1(x, y)$, defined by D_1 and s. It was used as the initial condition in modelling the high-temperature annealing process.

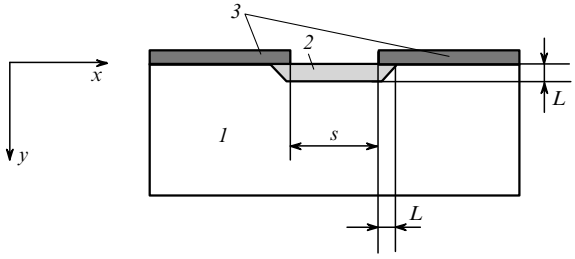

Figure 3. Model proton distribution in a waveguide after the first diffusion step: (*1*) lithium niobate substrate; (*2*) hydrogen-enriched zone; (*3*) metal mask.

In the second step of our simplified model, the hydrogen ion distribution $X(x, y)$ varies according to the diffusion equation with an effective mean diffusion coefficient D_2, which is independent of the hydrogen ion concentration:

$$\frac{\partial X(x, y)}{\partial t} = D_2 \nabla^2 X(x, y). \tag{2}$$

Given that the diffusion depth is much smaller than the substrate thickness, the substrate can be regarded as a semiplane. The initial condition has the form $X(x, y)|_{t=0} = X_1(x, y)$. The boundary condition at the substrate–air interface is that the ion flow from the substrate be zero. The solution to Eqn (2) for the semiplane with this condition is equivalent to the solution for the entire plane formed by the substrate semiplane and its reflection over the interface. To numerically solve Eqn (2), each grid node is thought of as a point source of protons, with a diffusion-induced proton distribution around it. The solution to Eqn (2) represents the hydrogen ion concentration at the nodes $X_2(x, y)$, which is a superposition of the proton distributions for all the point sources.

The hydrogen profile thus obtained was converted to the index difference profile (Fig. 4) using the formulas [9]:

$$X \leqslant 0.12, \quad \Delta n = 0.1623X, \tag{3}$$

$$0.12 < X < 0.56, \quad \Delta n = 0.3636X - 0.2656x^2 - 0.0203, \tag{4}$$

$$X > 0.56, \quad \Delta n = 0.0833X + 0.0533. \tag{5}$$

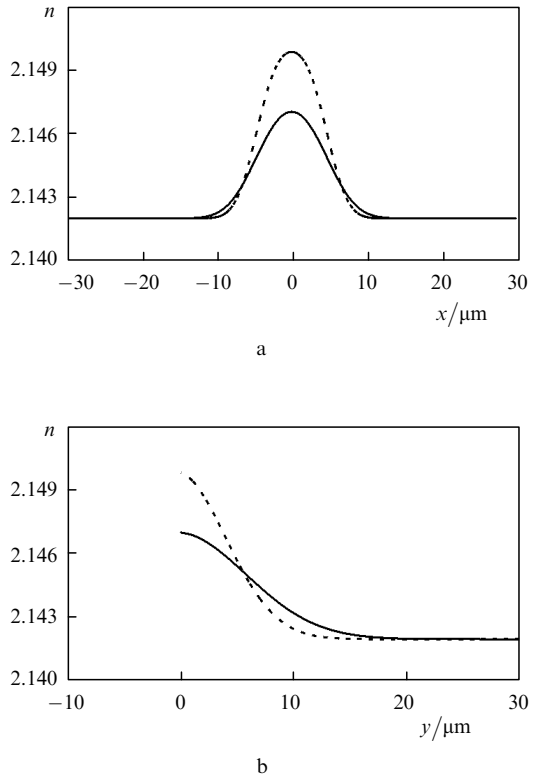

Figure 4. Calculated refractive-index (a) width and (b) depth profiles in the waveguide region after post-exchange anneals for 2 and 4 h (dashed and solid lines, respectively); $D_1 = 0.031$ μm h^{-1}, $D_2 = 1.2$ μm h^{-1}, slit width of 8.2 μm and proton exchange time of 20 min.

From the 2D index distribution, one can calculate the field distribution $U_i(x, y)$ for the fundamental mode of the optical waveguide using the finite difference method.

Waveguide modes are commonly calculated using an approximation that consists in numerically solving scalar wave equations for two orthogonal polarisations of a transverse electromagnetic wave. This approach is used to analyse weakly guiding waveguides, in which the index difference between the channel core and cladding is small, and the index gradient can be neglected. The structure under consideration has a sharp substrate–air interface, with a

jump in the refractive index, so the use of numerical solutions to scalar wave equations will lead to large computational errors.

In this study, to find eigenmodes we use a modified finite difference method in vector form. The eigenmodes of a waveguide are sought in the form of a propagating wave,

$$\hat{U}_i(x,y,z,t) = U_i(x,y)\exp[-\mathrm{i}(\beta z - \omega t)], \tag{6}$$

where $\hat{U}_i$ is one of the electromagnetic field components; β is the propagation constant of the fundamental model; and ω is the wave frequency.

Maxwell's equations for four $U_i(x,y)$ field components (two orthogonal electric field components, $U_1 = E_x$ и $U_2 = E_y$, and two orthogonal magnetic field components, $U_3 = H_x$ и $U_4 = H_y$) at each node have the form

$$N_{\mathrm{eff}}E_x = -H_y$$

$$-\left(\frac{1}{\varepsilon}\frac{\partial^2 H_y}{\partial x^2} + \frac{1}{\varepsilon}\frac{\partial^2 H_x}{\partial x \partial y} + \frac{\partial \varepsilon}{\partial x}\frac{\partial H_x}{\partial y} - \frac{\partial \varepsilon}{\partial x}\frac{\partial H_y}{\partial x}\right)\frac{1}{k^2},$$

$$N_{\mathrm{eff}}E_y = H_x$$

$$+\left(\frac{1}{\varepsilon}\frac{\partial^2 H_x}{\partial y^2} - \frac{1}{\varepsilon}\frac{\partial^2 H_y}{\partial x \partial y} + \frac{\partial \varepsilon}{\partial y}\frac{\partial H_x}{\partial y} + \frac{\partial \varepsilon}{\partial y}\frac{\partial H_y}{\partial x}\right)\frac{1}{k^2}, \tag{7}$$

$$N_{\mathrm{eff}}H_x = \varepsilon E_y + \left(\frac{\partial^2 E_y}{\partial x^2} - \frac{\partial^2 E_x}{\partial x \partial y}\right)\frac{1}{k^2},$$

$$N_{\mathrm{eff}}H_y = -\varepsilon E_x - \left(\frac{\partial^2 E_x}{\partial y^2} + \frac{\partial^2 E_y}{\partial x \partial y}\right)\frac{1}{k^2},$$

where $N_{\mathrm{eff}} = \beta/k$ is the effective refractive index of the mode; ε is the local, node-dependent permittivity; and $k = \omega/c$ is the wavenumber. The longitudinal field components E_z and H_z in (7) can be expressed through the transverse components. The system of Maxwell's equations for the four transverse electromagnetic field components allows the problem of solving Eqn (7) to be reduced to the problem of finding the eigenvalues and eigenvectors of a linear system of equations. In numerical methods, derivatives of field components with respect to coordinates are replaced by the differences between these components at neighbouring grid nodes. We obtain a system of linear equations in the vector $\boldsymbol{U}$, whose components are the electromagnetic field components at all the nodes. The length of the vector is $4N_{\mathrm{g}}$, where N_{g} is the number of nodes. For a 300×300 node grid, the vector length is 360000. The system can be written in the form

$$\hat{A}\boldsymbol{U} = \lambda \boldsymbol{U}, \tag{8}$$

where the linear operator $\hat{A}$ has the form of a banded matrix with eigenvalues

$$\lambda = (n_{\mathrm{wg}} - N_{\mathrm{eff}})/n_{\mathrm{wg}}. \tag{9}$$

Here, n_{wg} is the highest refractive index in the grid. In the system of linear equations (8), the diagonal elements of matrix $\hat{A}$ are the largest in magnitude, and the eigenvalues are in the vicinity of zero. Thus, to the fundamental mode of a waveguide corresponds the vector with the smallest in magnitude eigenvalue. This vector can be found using inverse iteration [10]. In this method, one calculates the vector $\boldsymbol{U}_N = -\hat{A}^{-N}\boldsymbol{U}_0$, where the initial approximation $\boldsymbol{U}_0$ is an arbitrary vector, and N is the number of iterations. In each iteration cycle, $\boldsymbol{U}_N = \hat{A}^{-1}\boldsymbol{U}_{N-1}$ is calculated by the Jacobi iterative method with M iterations. The initial approximation for the Jacobi method is the vector $\lambda_{N-1}^{-1}\boldsymbol{U}_{N-1}$. Thus, the eigenvector calculation involves MN iterations ($\sim$10000). In each inverse iteration step, we calculated the eigenvalue $\lambda_N = \boldsymbol{U}_N\boldsymbol{U}_{N-1}/\boldsymbol{U}_N^2$. When the number of inverse iterations exceeded 10000, the accuracy in the eigenvalues obtained was $\sim 10^{-4}$.

The eigenvector thus found is a set of electric and magnetic field components of the fundamental mode at the nodes and can be used to calculate the light intensity.

Thus, using numerical simulation we find the intensity distribution of the eigenmode in the cross section of the waveguide (Fig. 5). The shape of the calculated distribution

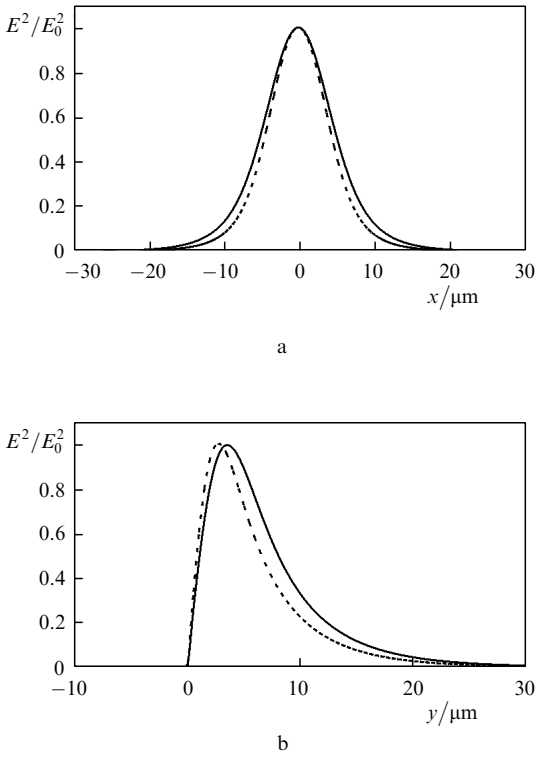

Figure 5. Calculated intensity distributions of the eigenmode of a waveguide in the (a) width and (b) thickness directions; post-exchange anneal for 2 and 4 h (dashed and solid lines, respectively); the other parameters are the same as in Fig. 4.

depends on proton exchange parameters: the slit width s in the mask and diffusion coefficients D_1 and D_2. The distribution can be used to determine the mode width and depth at a $1/e^2$ level and to compare them with experimental data. In comparing numerical simulation results with experimental data, D_1 and D_2 are used as adjustable parameters.

The proposed model allows one to examine the influence of process parameters, such as the proton exchange time, anneal time and slit width in the mask, on the depth and width of the intensity distribution across the fundamental mode. After defining the coefficients D_1 and D_2, one can tune the waveguide fabrication parameters and, accordingly, control the mode profile.

4. Discussion

The process parameters were initially chosen based on a systematic analysis of the literature on the fabrication of waveguides matched to SMF-28 standard single-mode fibre. Figure 6 shows the waveguide mode width and depth as functions of the slit width at two high-temperature anneal times (proton exchange time, 20 min). At an anneal time of 2 h and $s < 5$ μm, the waveguides do not support the fundamental mode at 1550 nm: we observe so-called cutoff, characteristic of waveguides with asymmetric boundary conditions. Increasing s to 7 μm decreases the mode width from 15 to 10.5 μm. This range corresponds to weakly guiding waveguides near cutoff. At higher s values, the mode width varies insignificantly. The mode depth varies with slit width in a similar way.

Annealing for another 2 h (a total of 4 h) increases the mode dimensions (as compared to 2-h annealing) at a given slit width, which is due to the diffusion broadening of the hydrogen-enriched zone. Note that, in the region where the mode dimensions strongly depend on s (weakly guiding waveguides near cutoff), the width of the waveguide mode coincides with its depth at a certain slit width. For example, our experimental data indicate that, at a net anneal time of 4 h and $s = 6$ μm, the mode width and depth are 17 μm.

In the above model, the diffusion coefficients D_1 and D_2 were fitting parameters. In this way, we calculated the width and depth of the intensity distribution in the waveguide mode as functions of the slit width at the process parameters corresponding to the experimental curves. The key point in determining the fitting parameters is to achieve agreement between the cutoff conditions at the experimentally determined slit widths. Good agreement between the calculation results and experimental data, including cutoff, was obtained at $D_1 = 0.031$ μm h^{-1} and $D_2 = 1.2$ μm h^{-1} (Fig. 6).

These values of D_1 and D_2, obtained for the samples proton-exchanged for 20 min, were used to calculate the waveguide mode width and depth as functions of slit width at a proton exchange time of 50 min and post-exchange anneal time of 4 h (Fig. 7). From the above model, it is clear

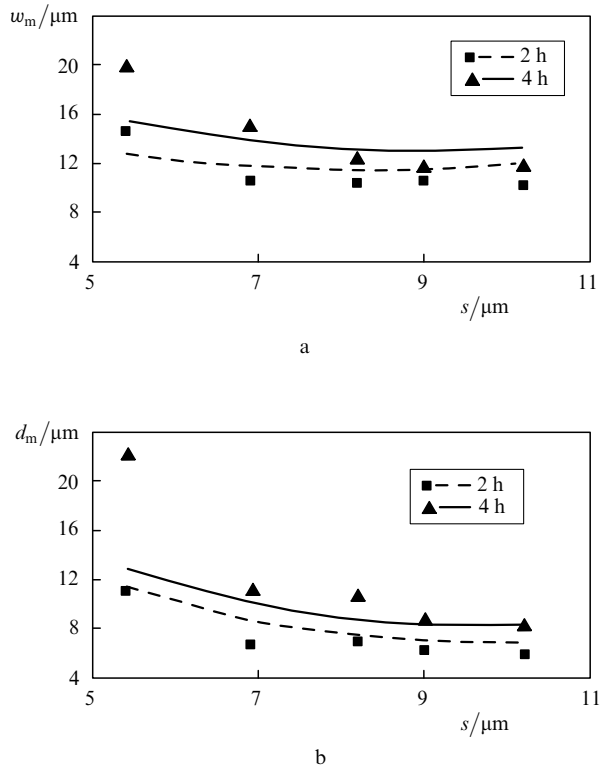

Figure 6. Measured (points) and calculated (curves) waveguide mode (a) width and (b) depth as functions of the slit width in the mask at two post-exchange anneal times; $D_1 = 0.031$ μm h^{-1}, $D_2 = 1.2$ μm h^{-1}, proton exchange time of 20 min.

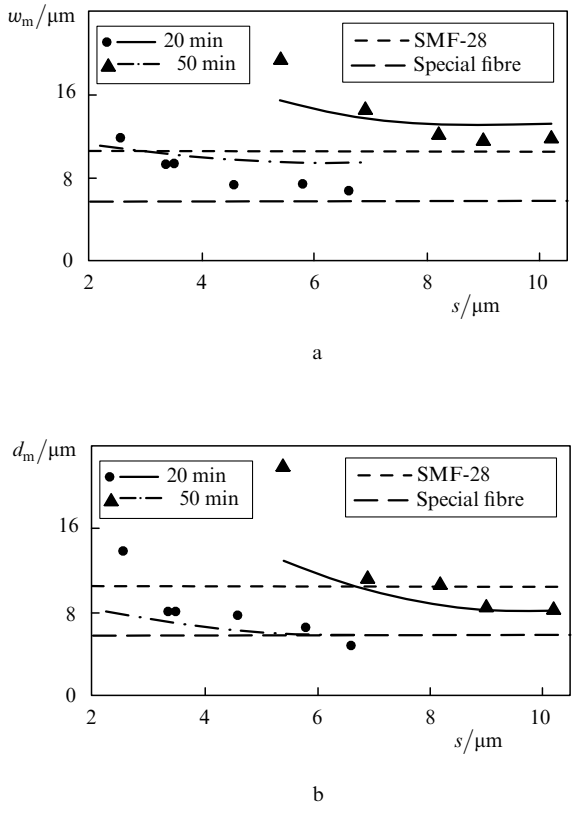

Figure 7. Measured (points) and calculated (curves) waveguide mode (a) width and (b) depth as functions of the slit width in the mask at two proton exchange times; $D_1 = 0.031$ μm h^{-1}, $D_2 = 1.2$ μm h^{-1}, post-exchange anneal time of 4 h. The dashed horizontal lines, corresponding to the SMF-28 and a special fibre, illustrate the degree of mode matching.

that increasing the proton exchange time must increase the amount of protons incorporated into the substrate. All other process parameters being the same, this would eventually lead to an increase in the refractive index of the channel and, hence, to stronger wave localisation and a reduction in the effective mode width and depth.

As seen in Fig. 7, the calculation results agree well with the experimental data. In accordance with theoretical predictions, increasing the proton exchange time from 20 to 50 min, without varying the other process variables, considerably reduces the waveguide mode dimensions. Moreover, at the longer proton exchange time no cutoff occurs, even at $s = 2.5$ μm (mode width of 12 μm and depth of 14 μm). For $s > 4$ μm, the mode dimensions vary only slightly with slit width. For $s > 7$ μm, the waveguide supports two or more modes at $\lambda = 1550$ nm, in accordance with theoretical predictions.

The results of our experimental and theoretical studies into the effect of process parameters on the mode dimensions in annealed proton-exchanged channel waveguides demonstrate that the slit width in the mask offers an additional means of controlling the characteristics of waveguides, in particular, the parameters of the waveguide mode. All other process parameters being the same, the cross-sectional dimensions of the waveguide mode may vary from 20 to 5 μm in response to changes in the slit width. Another important implication is that the slit width influences both the width and depth of the mode. Analysis of our experimental data in conjunction with the above simplified model suggests that, at process parameters typical of the fabrication of single-mode waveguides free of electrooptical degradation, it is the net amount of hydrogen incorporated into the lithium niobate substrate as a result of proton exchange (first processing step) which determines the largest index change in the waveguide channel. The hydrogen content, in turn, depends on the proton exchange time and temperature and the slit width (with increasing slit width, the proton exchange area increases, and more hydrogen is incorporated into the substrate).

Analysis of the present experimental data suggests that, in the region where the mode dimensions strongly depend on slit width (weakly guiding waveguides near cutoff), one can choose a slit width such that the waveguide will have a nearly symmetric mode. At the same time, even slight deviations from the necessary process parameters will lead to a large error in mode dimensions.

Our results indicate that there are certain waveguide fabrication conditions under which the characteristics of the waveguide mode are insensitive to variations in slit width in the range $\pm(1 \div 1.5)$ μm. This is of practical importance because, as a result, the characteristics of integrated optical devices are weakly influenced by fabrication errors in the photolithography step, which is essential for large-scale production.

To ensure good mode match to a standard SMF-28 telecommunication fibre, the slit width must be $s = 8 - 10$ μm, proton exchange must be performed for 20 min at 200 °C, and post-exchange anneal, for 4 h at 350 °C. The measured width and depth of such waveguides are $w_m = 11.8 - 12.4$ μm and $d_m = 8.2 - 10.8$ μm. For a Gaussian mode with $w_m = 12$ μm and $d_m = 9$μm, the estimated waveguide to SMF-28 coupling loss is 0.21 dB per fibre-to-waveguide connection. This estimate is rather rough because the actual intensity distribution in guided modes is far from being Gaussian (especially along the vertical axis). The measured overall fibre-to-fibre loss for a sample with two connections was 2.5 dB. Note that this value includes, in addition to the coupling loss, the Fresnel reflection loss at the end-faces and the intrinsic waveguide loss. To ensure match to a special fibre (5.8-μm-diameter core), we used a waveguide fabricated under the following conditions: proton exchange for 50 min at 200 °C, post-exchange anneal for 4 h at 350 °C and $s = 4.5 - 6.5$ μm. The mode dimensions in such waveguides are $w_m = 6.8 - 7.4$ μm and $d_m = 4.6 - 7.6$ μm, and the theoretically predicted coupling loss at $w_m = 6.8$ μm and $d_m = 4.6$ μm is 0.25 dB.

5. Conclusions

The influence of low-temperature proton exchange conditions on the mode profile of lithium niobate channel waveguides was studied experimentally and theoretically. The fabrication conditions were such that the waveguides had good electro-optical properties, similar to those of bulk crystals. The effect of the slit width in the mask on the mode profile was examined. The results indicate that, in the case of proton-exchanged waveguides, the slit width influences both the width and depth of the guided mode and, hence, offers an additional means of tuning the mode profile. At the same time, in the fabrication of waveguides via low-temperature proton exchange followed by annealing there are certain process conditions at which the mode dimensions are insensitive to variations in the slit width in the range $\pm(1 \div 1.5)$ μm. Such conditions ensure high stability towards fabrication errors, especially in the photolithography step. The proposed simplified model helps to optimise waveguide fabrication parameters in order to control the mode profile and to meet the performance requirements of integrated optical devices. The theoretical analysis results agree well with experimental data.

Acknowledgements. The authors thank M.P. Petrov for his invaluable assistance with this study.

References

1. Jackel J.L., Rice C.E., Veselka J.J. *Appl. Phys. Lett.*, **41**, 607 (1982).
2. Korkishko Y.N., Fedorov V.A. *In ion exchange in single crystal for integrated optics and optoelectronics* (Cambridge: Cambridge International Sci. Publ, 1999) p. 97.
3. Korkishko Y.N., Fedorov V.A. *Zh. Tekhn. Fiz.*, **69** (3), 47 (1999).
4. Bortz M.L., Eyres L.A., Fejer M.M. *Appl. Phys. Lett.*, **62**, 2012 (1993).
5. Suchoski P.G., Findakly T.K., Leonberger F.J. *Opt. Lett.*, **13**, 1050 (1988).
6. Korkishko Yu.N., Fedorov V.A. *Kristallografiya*, **44**, 271 (1999).
7. Mendez A., de la Paliza G., Garcia-Cabanes A., Cabrera J.M. *Appl. Phys. B.*, **73**, 485 (2001).
8. Espeso O., Garcia G., Climent A., Agullo-Lopez F., de la Paliza G., Cabrera J.M., Sajavaara T. *J. Appl. Phys.*, **94**, 7710 (2003).

9. Torben Veng, Torben Skettrup. *J. Lightwave Techn.*, **16**, 646 (1998).
10. Faddeev D.K., Faddeeva V.N. *Vychislitel'nye metody lineinoi algebry* (Computational Methods of Linear Algebra) (Moscow: Lan', 2002).